GEOPHYSICAL RESEARCH LETTERS, VOL. 28, NO. 16, PAGES 3183-3186, AUGUST 15, 2001

Eddies and vortices in ocean basin dynamics

A. Siegel[1,6], Jeffrey B. Weiss[1], Juri Toomre[2], James C. McWilliams[3,4], Pavel S. Berloff[3], and Irad Yavneh[5]

Abstract. A wind-driven, closed-basin quasi-geostrophic ocean model is computed at very high horizontal resolution to study the effect of increasing Reynolds number (Re) on eddy variability. Five numerical simulations are performed with identical configurations, varying only in horizontal resolution and viscosity coefficient (and therefore Re). Qualitative changes in the structure of eddy variability are evident in the dramatic increase of isolated vortex structures at the highest Re. While the time-mean kinetic energy is relatively independent of Re, the vortex emergence contributes to a continual increase with Re of eddy kinetic energy and meridional vorticity flux. The rate of increase slows somewhat at the highest Re, indicating the possibility of a regime where eddy variability becomes insensitive to further increases in Re.

Introduction

Properly diagnosing oceanic transport is crucial for the development of accurate climate models. Unfortunately, even state-of-the-art Ocean General Circulation Models (OGCM's) show little evidence of large-scale resolution convergence – that is, gross oceanic features have not tended to a roughly constant state with increasing Re [*Treguier*, 1992; *Semtner*, 1992; *Smith et al.*, 1998; *Bryan*, 1996; *Covey*, 1995; *Drijfhout*, 1994; *Gent and McWilliams*, 1996].

In this note we explain preliminary results from a set of numerical experiments performed at unprecedented resolution designed to shed light on the very high-Re behavior of ocean basin simulations. We address this problem in the context of the simplified and computationally less intensive quasigeostrophic (QG) equations in a geometrically idealized box domain (e.g., see Holland [1978]). This permits us to perform simulations over a range of previously unexplored grid resolutions and for the multi-year time intervals required to understand statistical trends. The discussion presented here is intended as a first look at some novel aspects of these solutions and their implications for ocean modelling. More detailed analyses of these idealized solutions can then be used to guide the development of subgrid parameterizations for more realistic models.

[1]Program in Atmospheric and Oceanic Sciences, University of Colorado, Boulder, CO

[2]JILA, University of Colorado, Boulder, CO

[3]Department of Atmospheric Sciences, UCLA, Los Angeles, CA

[4]Also at National Center for Atmospheric Research, Boulder, CO

[5]Technion, Israel Institute of Technology, Department of Computer Sciences, Haifa, Israel

[6]Currently at ASCI Flash Center, University of Chicago

Paper number 1999GL011246.
0094-8276/01/1999GL011246$05.00

Numerical Simulations

We carry out our investigations using the wind-driven QG equations solved with very high horizontal resolution on a shallow, square domain of dimension $3200 \times 3200 \times 5$ km. The simulations use asymmetric winds to force a double-gyre circulation on a beta plane, centered at $\theta_0 \sim 40^\circ$ North latitude, with bottom friction and no-slip, impermeable side boundaries. Subgrid effects are modelled by Newtonian dissipation in the horizontal, with no inter-layer vertical diffusion. Details of the vertical structure are identical to the six-level experiments of Barnier [1991]. A series of five numerical simulations is performed covering a range of Re but with otherwise identical configurations. The largest simulation has a horizontal resolution approximately five times greater than current OGCM's. The parameters are stated in Table 1.

All computations are performed on Cray T3E at the San Diego Supercomputer Center, using as many as 128 simultaneous processors. The numerical method is explicit predictor-corrector in time and multigrid in space, similar to Yavneh and McWilliams [1996]. All but the highest resolution simulations are integrated for at least 15 years of model time to arrive at a state of statistical equilibrium, at which point an additional 7 year run is conducted. For r1.6 (see Table 1), a total of 9 years is computed using an equilibrated solution from r3.1 as an initial condition. In this case, the final 3 years are used for statistical analysis.

Eddy Structure

At sufficiently high Re, the double-gyre flows develop transient motions sustained by velocity shear in the mean circulation. After the initial spin-up phase, a statistical equilibrium is established between mean and eddy fields. Thus, the dependence of the time–mean flow patterns on Re suggests corresponding changes in eddy variability. We focus here on the spatial organization of the eddy field. Oceanic observation reveals a great variety of coastal and interior mesoscale and submesoscale vortex processes which are only partially reproduced in OGCM's. One possible explanation is inadequate horizontal resolution, which dampens vortex-forming instabilities. We qualitatively measure the effect of Re on eddy structure through visualizations of the relative potential vorticity q_r, defined as

$$q_r = \nabla_h^2 \psi + \frac{\partial}{\partial z} S^{-1} \frac{\partial \psi}{\partial z}, \qquad (1)$$

where ψ is the streamfunction and $S(z)$ the stability parameter, z the vertical coordinate, and $\nabla_h^2 \equiv \frac{\partial^2}{\partial x^2} + \frac{\partial^2}{\partial y^2}$.

Instantaneous images of the upper-level q_r field are shown in Plate 1. At low Re, amorphous wave-like patterns of transient motions are evident (Plate 1A). As Re is increased, vortices begin to emerge (Plate 1B). Computer animations reveal that the vortices mainly originate as 'rings', which evolve from jet meanders that form closed loops and pinch

off elliptical structures. The rings evident in Plate 1B have diameters of order 100 km and lifetimes of several months, limited by their re-absorption into the jet, merging with other rings, or irreversible deformation by large-scale strain after viscous weakening. Vortices are also observed to form sporadically in the southern half of the western boundary current (WBC), being advected northward and subsequently annihilated by the strong shear present near the boundaries of the interior jet.

These short lifetimes and small populations of vortices are inconsistent with observation. For example, Gulf Stream rings often persist for several years and maintain temperature and chemical properties distinct from the surrounding ocean *Chassignet* [1992]. Isolated vortices, self-advecting mushroom dipoles, submesoscale coherent structures, and coastal vortex shedding also have been observed to a greater extent than what these results indicate.

However, case r6.25 reveals a more numerous and well-defined vortex population, particularly in the vicinity of the offshore jets (Plate 1C). Coherent structures immediately north and south of the main jet typically span 100 – 200 km in diameter. Their lifetimes range from 100 – 200 days, following a cycle of creation from jet meanders, slow westward propagation, and ultimately re-incorporation into the WBC. About half of the vortices are annihilated prematurely by fluctuations in the jet or collisions with other rings. Among the vortices which survive, a small number cross into the northern gyre. From $0 < Y < 700$ km, eddy fluxes show an increased tendency to organize into structures, but even the strongest vortices still survive $\sim$ 20 days. At the southern/northern boundaries, positive/negative PV anomalies created in the viscous sublayer are evident. Flow animations reveal that these vortices are quickly swept into the boundary currents and do no penetrate into the interior flow.

At r3.25 and r1.65, vortex structures covering a wide range of scales populate most of the region south of main jet. Submesoscale vortices as small as 10 km penetrate the interior flow on the southern, northern, and western boundaries and frequently endure for over a year. In the same regions, vortices which 'roll-up' spontaneously from small-scales perturbations in the turbulent boundary layers show much greater resilience as they are slowly carried westward by the broad return flow. Near the jet, vortex rings are spawned and interact with the interior vortices, both as same and opposite sign vortex mergers which spawn filaments and dissipate enstrophy. Direct vortex-vortex mergers, which are frequent and conspicuous in flow animations, become increasingly common and limit the growth of the population [*McWilliams et al.*, 1999; *Weiss and McWilliams*, 1993; *von Hardenberg et al.*, 1999]. In r3.25, meandering vortices at times have enough inertia to cross the westward return flow

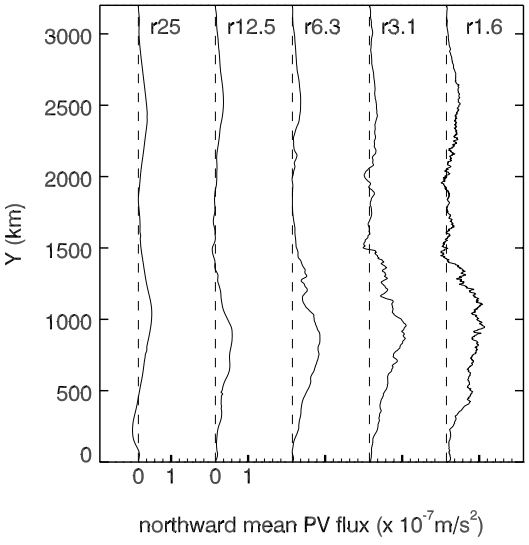

Figure 1. Variation with latitude of northward upper-level mean potential vorticity transport for each simulation, with each curve displaced to the right for clarity. The transports are derived from longitudinal averages of the flow. The amplitude of the profiles increases slightly with Re, but their overall shape is remarkably similar.

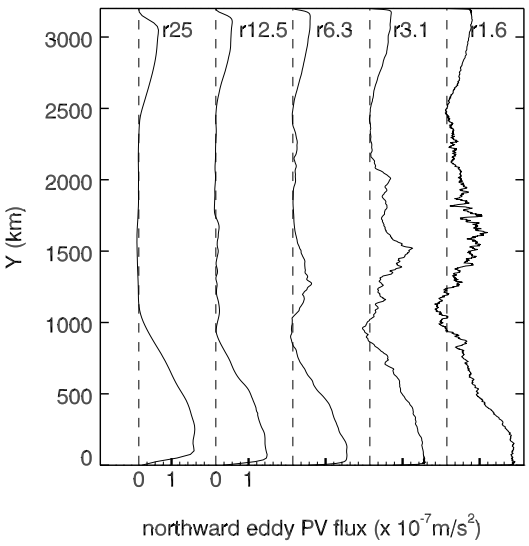

Figure 2. As in Fig. 1, showing variation of northward upper-level eddy potential vorticity transport with lattitude for each simulation. Strong eddy variability develops at high Re in regions where the jet persists, due to both jet undulations and the presence of coherent vortex structures.

Table 1. Non-constant parameters for the five numerical experiments discussed in the text. These involve increasingly finer horizontal resolution and reduced viscosity, yielding a wide range of Sverdrup Re. All experiments use six grid points in a box of dimension $3200 \times 3200 \times 5$ km, with mean layer thicknesses $H = [2100, 1350, 500, 350, 300, 250]m$, interfacial reduced gravities $g' = [1.17, 4.99, 5.24, 8.08, 12.0] \times 10^{-3} m^2 s^{-2}$, $\beta_0 = 10^{-11} m^{-1} s^{-1}$, $f_0 = 9.3 \times 10^{-5} s^{-1}$, bottom friction spindown rate $r = 10^{-7} s^{-1}$, kinematic wind stress amplitude $\tau_0 = .6 \times 10^{-4} m^2 s^{-2}$. Since the Sverdrup velocity is only of order 10^{-3} ms^{-1}, the values of Re seem unusually small. It must be kept in mind that these values are physically representative of the basin interior far from the offshore jets, and that jet-based values of Re are approximately three orders of magnitude larger.

Label	δx	horiz. grid points	$\nu m^2/s^2$	Re
r25.0	25.0	128×128	1600	.375
r12.5	12.5	256×256	400	1.50
r6.3	6.25	512×512	100	6.00
r3.1	3.12	1024×1024	25	24.00
r1.6	1.56	2048×2048	6.25	96.00

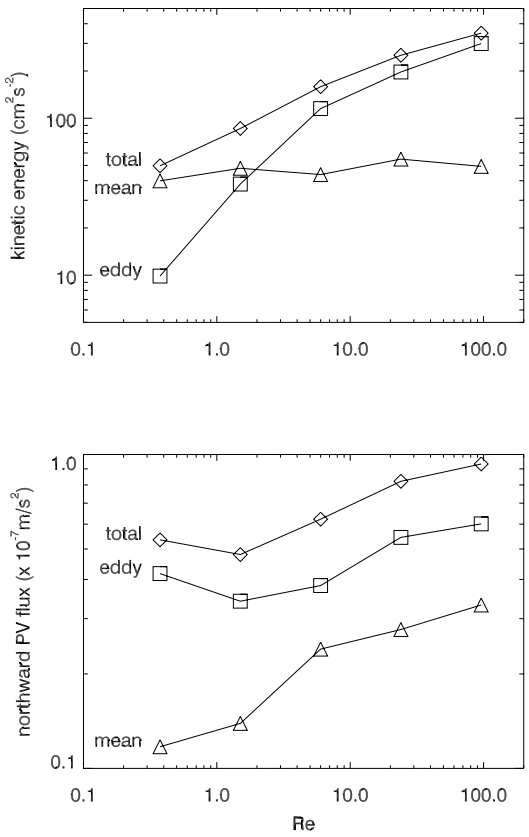

Figure 3. Upper-level averaged (A) kinetic energy and (B) northward potential vorticity flux for the five simulations, as a function of Re. The mean and eddy components are shown together with their totals. (A) the mean values have no clear trend across the entire range of Re. (B) both the mean and the eddy components show some indication that their rate of increase is slowing at the highest Re.

and transport their material contents northward across the gyre. This is more common in r1.65, when a second jet is not present (see Plate 2E) to absorb the northward-propagating vortices, contributing to large values of eddy PV flux north of the mean jet latitude.

Eddy Statistics

The explosion of small and mesoscale structure at higher Re is of potential significance for the development of subgrid models. Similar vortex behavior has been observed extensively in idealized 2-D simulations [*McWilliams*, 1990], which have shown that the long-lived coherent structures complicate attempts to use simple diffusive eddy–mean flow relations. In the present study we are particularly interested in some simple quantitative measures of the variation of the eddy field with Re, to which the vortices necessarily contribute. Thus we compute eddy–mean field statistics for the pointwise kinetic energy (KE) and northward potential vorticity transport. Denoting the time–average (overbar) and fluctuating (primed) variables, we compute:

$$\overline{u^2+v^2} = (\overline{u}^2+\overline{v}^2)+(\overline{u'^2}+\overline{v'^2}) \quad (2)$$

$$\overline{vq} = \overline{v}\,\overline{q}+\overline{v'q'} \quad (3)$$

where u and v are the eastward and northward horizontal velocity components and q represents the absolute potential vorticity (i.e. $q = q_r + \beta y$).

Eddy Kinetic Energy In examining upper-level EKE maps (not shown), we find that the spatial variations of EKE at low Re greatly underestimate observation. A similar failure of OGCM's to accurately mimic observed levels of EKE has long been recognized as a fundamental shortcoming [*Treguier*, 1992; *Semtner*, 1992; *Smith et al.*, 1998; *Maltrud et al.*, 1998]. Experiments indicate that values of EKE are far higher than those present in eddy-resolving OGCM's, even when resolution is increased to 1/6° (as a rough guide, 1/6° resolution corresponds to r12.5 in Table 1) [*Wilkin and Morrow*, 1994; *Beckmann et al.*, 1993]. The 1/6° simulations show some improvement over the corresponding 1/3° calculations, suggesting that the model deficiencies are due at least in part to insufficient resolution. Further improvement is shown when resolution is refined to 1/10° [*Bryan and Smith*, 1999]. Overall distributions of EKE tend to be fairly realistic in these models, but intensity levels are still underestimated, particularly in the interior regions [*Treguier*, 1992; *Stammer and Boning*, 1991; *Beckmann et al.*, 1993].

Our QG solutions provide some rough insight into the role of resolution alone in determining typical EKE values. At low Re, maximum values occur in the vicinity of the jet but do not exceed 0.1 m^2/s^2, and in the eastern part of the basin values are typically of order 10^{-4} m^2/s^2. As with OGCM's, these latter values fall far short of oceanic esti-

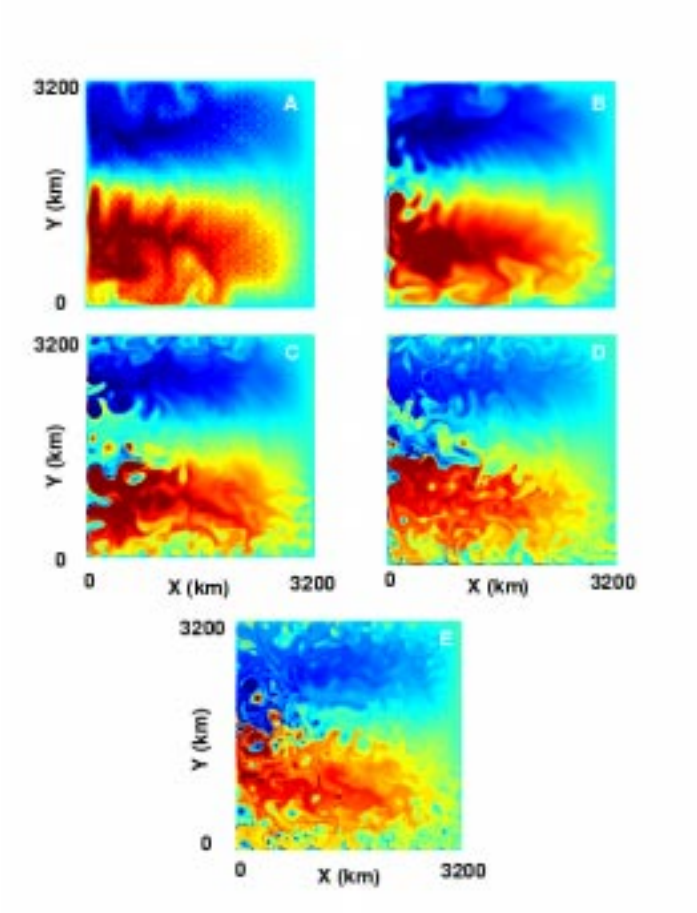

Plate 1. Upper-layer potential vorticity (PV), with positive and negative extrema represented by blue and red, respectively. Shown are resolution of A) 25km (128 x 128), B) 12.5km (256 x 256), C) 6.25km (512 x 512), D) 3.12km (1024 x 1024), and E) 1.56km (2048 x 2048).

mates [*Treguier*, 1992]. However, higher resolution itself appears capable of producing more realistic levels of variability, with maximum amplitudes approach 0.25 m^2/s^2, and values as high as 0.01 m^2/s^2 in the eastern half of the basin.

Potential vorticity fluxes The northward fluxes of q give a general sense of the poleward transport of material fluid elements. Figure 1 shows the latitudinal variation of the mean q flux, and Figure 2 the eddy q flux, each obtained by a longitudinal average. The mean flux profiles possess similar spatial structure, increasing slightly in amplitude as Re increases. The eddy component shows larger variation of Re, with a prominent increase near the center of the basin as Re increases. This behavior arises from meanderings and fluctuations of the main jet, and from the continuous generation of the coherent vortices which emerge in the vicinity of the jet. Near the southern boundary, eddy q transport is relatively invariant among the five simulations — vortices form spontaneously near the southern wall in the highest Re cases, but apparently do not enhance transport on average.

Basin-averaged quantities Finally, we compare global averages of the total, mean, and eddy components of the KE (Figure 3A) and q fluxes (Fig. 3B) for the five simulations. The mean kinetic energy (MKE) varies by less than thirty percent and shows no discernible trend with increasing Re, whereas the EKE increases from about half to more than ten times the MKE. At the highest Re the EKE values approach oceanic measurements. The basin-averaged q fluxes show increases in both the eddy and mean components, with the relative proportion of the eddy component to the mean decreasing slightly with Re. Our primary interest is the asymptotic behavior of these curves in order to determine whether the increase in the EKE and eddy q fluxes with Re is likely to continue. Fig. 3A-B do not unambiguously indicate that the eddy processes are approaching an asymptotically invariant regime, though in Fig. 3B in particular there is basis for optimism that such a regime may exist at higher Re.

Conclusion

By comparing simulations covering a large range of Re we have been able to gain important insight into the behavior of mesoscale processes in the ocean. The set of simulations is highly idealized, but the simplifications allow us to compute at significantly higher Re than has been possible with full OGCM's. Basic features of the large-scale gyre structure and MKE appear to be relatively insensitive to Re, while the EKE and northward q fluxes increase and approach observed oceanic values. The rate of increase slows somewhat with Re, indicating the possible existence of a regime at even higher Re where the eddy/mean balances become roughly independent of Re. This increased eddy activity is related in part to a growing vortex population reminiscent of the rich variety of coherent mesoscale structures observed in oceanic satellite imagery. These features are not observed in lower Re simulations, and we are confident that an understanding of their emergence and dynamics is crucial for the development of parameterizations for OGCM's with coarser grids.

Acknowledgments. The authors acknowledge partial support by National Science Foundation grants GER-9355046, ESC-9217394, and OCE-9818839.

References

Barnier, B., B. L. Hua, and C. Le Provost, On the catalytic role of high baroclinic modes in eddy-driven large-scale circulations, *J. Phys. Oceanogr.*, 21(7), 976–997, 1991.

Beckmann, A., C. Koberle, and J. Willebrand, Effects of increased horizontal resolution in a simulation of the North Atlantic Ocean, *J. Phys. Oceanogr.*, 24(2), 326–344, 1993.

Bryan, F. and R. D. Smith,, Modelling the North Atlantic circulation: from eddy-permitting to eddy-resolving, *WOCE Newsletter*, 33, 12–14, 1999.

Bryan, K., The role of mesoscale eddies in the poleward transport of heat by the oceans: a review, *Physica D*, 98(2–4), 249–257, 1996.

Chassignet, E., Rings in numerical models of ocean general circulation: a statistical study, *J. Geophys. Res.*, 97(C6), 9479–92, 1992.

Covey, C., Global ocean circulation and equator-pole heat transport as a function of ocean GCM resolution, *Climate Dynamics*, 11,425–437, 1995.

Drijfhout, S. S., Heat transport by meoscale eddies in an ocean circulation model, *J. Phys. Oceanogr.*, 24(2), 353–369, 1994.

Gent, P. and J. McWilliams, Eliassen-Palm fluxes and the momentum equations in non-eddy-resolving ocean circulation models, *J. Phys. Oceanogr.*, 26(11),2539–46, 1996.

Holland, W. R., The role of mesoscale eddies in the general circulation of the ocean—numerical experiments using a wind-driven quasi-geostrophic model, *J. Phys. Oceanogr.*, 8(3), 363–92, 1978.

Maltrud, M., R. Smith, A. Semtner, and R. Malone, Global eddy-resolving ocean simulations driven by 1985-1994 atmospheric winds, *J. Geophys. Res.*, 103(C13), 30825–53, 1998.

McWilliams, J. C., The vortices of two-dimensional turbulence, *J. Fluid Mech.*, 219, 361–85, 1990.

McWilliams, J. C., J. B. Weiss, and I. Yavneh, The vortices of homogeneous geostrophic turbulence *J. Fluid Mech.*, **401**, 1-26, (1999).

Semtner, A., Ocean general circulation from a global eddy-resolving model, *J. Geophys. Res.*, 97(C4), 5493–550, 1992.

Smith, R., M. Maltrud, M. Hecht, and F. Byran, Numerical simulations of the North Atlantic at 1/10 degree, *J. Phys. Oceanogr.*, submitted, 1998.

Stammer, D. and C. W. Boning, Mesoscale variability in the atlantic ocean from GEOSAT altimetry and WOCE high-resolution numerical modelling, *J. Phys. Oceanogr.*, 22(7), 732–52, 1991.

Treguier, A. M., Kinetic energy analysis of an eddy resolving, primitive equation model of the North Atlantic, *J. Geophys. Res.*, 97(C1), 687–701, 1992.

Von Kardenberg, J, J.C. McWilliams, A. Provenzale, A. Shchepetkin, and J. B. Weiss, Vortex merging in quasigeostrophic flows, *J. Fluid Mech.*, submitted, 1999.

Weiss, J. B. and J. C. McWilliams, Temporal scaling behavior of decaying two-dimensional turbulence, *Phys. Fluids*, 5(3), 608–21, 1993.

Wilkin, J. L. and Morrow, R., Eddy kinetic energy and momentum flux in the Southern Ocean: Comparison of a global eddy-resolving model altimeter, drifter, and current-meter data, *J. Geophys. Res.*, 99(C4), 7903–16, 1994.

ASiegel and JB. Weiss,Program in Atmospheric and Oceanic Sciences, University of Colorado, CB 311, Boulder, CO 80309-0311. (email:jweiss@colorado.edu; siegela@flash.uchicago.edu)

J. Toomre, JILA, University of Colorado, CB 440, Boulder, CO 80309-0311. (e-mail:jtoomre@jila.colorado.edu)

J. C. McWilliams and P. S. Berloff, Department of Atmospheric Sciences, UCLA, Los Angeles CA 90095-1361. (e-mail:jcm@cisk.atmos.ucla.edu; pavel@cheyenne.atmos.ucla.edu)

I. Yavneh, Technion – Israel Institute of Technology, Department of Computer Sciences, Haifa, Israel.
(e-mail:irad@CS.technion.ac.il)

(Received November 15, 1999; revised July 5, 2000;
accepted July 5, 2000.)